processes

MDPI

Article

Additive Manufacturing via Direct Ink Writing of Customized Silicone Foam with Glycerol as Dispersed Phase for Diverse Applications

Kenrick Weiting Tie [1], Jia Huey Sim [2,3,*], Jing Yuen Tey [1,4], Wei Hong Yeo [1,4], Zhi Hua Lee [2,3], Law Yong Ng [2,3], Soo Tueen Bee [1,*], Tin Sin Lee [2] and Luqman Chuah Abdullah [5]

1 Department of Mechanical and Material Engineering, Lee Kong Chian Faculty of Engineering and Science, Universiti Tunku Abdul Rahman, Kajang 43000, Selangor, Malaysia; kenrick45@1utar.my (K.W.T.); teyjy@utar.edu.my (J.Y.T.); yeowh@utar.edu.my (W.H.Y.)
2 Department of Chemical Engineering, Lee Kong Chian Faculty of Engineering and Science, Universiti Tunku Abdul Rahman, Kajang 43000, Selangor, Malaysia; leezh@utar.edu.my (Z.H.L.); lyng@utar.edu.my (L.Y.N.); leets@utar.edu.my (T.S.L.)
3 Centre for Advanced and Sustainable Materials Research (CASMR), Universiti Tunku Abdul Rahman, Kajang 43000, Selangor, Malaysia
4 Centre for Sustainable Mobility Technologies (CSMT), Universiti Tunku Abdul Rahman, Kajang 43000, Selangor, Malaysia
5 Department of Chemical Engineering, Faculty of Engineering, Universiti Putra Malaysia, Serdang 43400, Selangor, Malaysia; chuah@upm.edu.my
* Correspondence: simjh@utar.edu.my (J.H.S.); beest@utar.edu.my (S.T.B.)

Abstract: Direct ink writing (DIW) enables the additive manufacturing of silicone elastomers, offering an alternative to traditional moulding and casting methods for applications from healthcare products to machine–human interaction sensors. Polydimethylsiloxane (PDMS) foam, a porous silicone elastomer, is valued for its elasticity, chemical and thermal resistance, hydrophobicity, and biocompatibility. The emulsion templating method is a simple and cost-effective approach to create silicone foams by incorporating and later removing a sacrificial dispersed phase from the PDMS precursor. This study developed glycerol/PDMS emulsion-based inks for DIW using high-shear centrifugal mixing, with ethanol as a solvent to remove the glycerol template, creating silicone foam. An optimal glycerol dosage of 50 parts per hundred rubber (phr) produced foam with 27.63% porosity and pore diameter up to 4.66 µm. Each 10 phr increase in glycerol content raised porosity by 10% and average pore diameter by 2 µm. Both tensile and compressive behaviour inversely correlated with porosity, with a 10% porosity rise in the silicone foam reducing tensile strength by 0.07 MPa and stiffness by 0.02 MPa. Models with strong data alignment were developed to benefit researchers in 3D printing to customize silicone foams (pore properties, mechanical properties, compressive properties) based on specific application requirements.

Keywords: silicone; 3D printing; direct ink writing

check for updates

Academic Editor: Diane Mynors

Received: 16 January 2025
Revised: 17 February 2025
Accepted: 24 February 2025
Published: 27 February 2025

Citation: Tie, K.W.; Sim, J.H.; Tey, J.Y.; Yeo, W.H.; Lee, Z.H.; Ng, L.Y.; Bee, S.T.; Lee, T.S.; Abdullah, L.C. Additive Manufacturing via Direct Ink Writing of Customized Silicone Foam with Glycerol as Dispersed Phase for Diverse Applications. *Processes* **2025**, *13*, 677. https://doi.org/10.3390/pr13030677

Copyright: © 2025 by the authors. Licensee MDPI, Basel, Switzerland. This article is an open access article distributed under the terms and conditions of the Creative Commons Attribution (CC BY) license (https://creativecommons.org/licenses/by/4.0/).

1. Introduction

Polydimethylsiloxane (PDMS) is a synthetically derived silicone polymer that comprises repeating siloxane (Si-O) monomers as the backbone, with two methyl groups (CH_3) bonded to each silicon atom [1]. The long bond lengths and large bond angles of the ionic Si-O groups account for the great flexibility of PDMS elastomers, while their high dissociation energy leads to their outstanding chemical and thermal stability [2,3]. The low intermolecular forces between nonpolar methyl groups instigates their hydrophobicity and

low surface tension [4]. Due to these characteristics, PDMS elastomers possess fantastic properties such as hydrophobicity, biocompatibility, corrosion resistance, great elasticity, gas permeability, dielectric properties, and so forth [5]. Hence, PDMSs are favoured in wide applications such as coatings, membranes, microfluidics, biomedical and tissue engineering, sensors, electrical devices, etc. [6].

Porous polymer structures have been exploited in numerous applications due to their unique properties and diverse functionality [7]. The porosity provides a high surface area to volume ratio, at the same time enhancing the flexibility of PDMS structures [8]. Since the inception of this concept, porous PDMSs have been meticulously developed as separation membranes [9]. Oil/water separation membranes are well-known examples due to escalated cases of water pollution [10]. Hence, porous PDMS membranes have been created, which are sustainable, reusable, cheap, and easy to produce [10–13].

Scaffolds for tissue engineering are another instance for the motive behind porous PDMS. There are prerequisites for these scaffolds, such as being biocompatible, mechanically robust, and porous. Porosity is vital as it impacts the surface available for cell adhesion, promoting cell growth, and, more importantly, provides access for nutrient transport and waste removal [14]. Porous PDMS scaffolds have been fabricated with different techniques [1,15–17], as it is the ideal material that satisfies these requirements [9].

In recent times, porous PDMSs have advanced into electronics such as wearable pressure sensor devices [18,19]. These sensors generally work by detecting the changes in resistance or capacitance when subjected to deformation [19,20]. Porous PDMS composites are preferred as they are light-weight, and display improved flexibility and deformability through reduced elastic modulus that allows them to react more accurately to changes in electrical properties [21]. A number of studies have induced porosity into the PDMS dielectric layer in order to boost sensitivity [19–24]. Therefore, introducing porosity into PDMS results in foams with altered properties that can be tuned to suit a variety of applications.

Porous PDMSs are manufactured with different strategies, such as gas foaming or templating methods [25]. Gas foaming adopts chemical blowing agents that release gaseous by-products into the foams, or physically injects these gases into the polymer melt. Due to templating methods being relatively basic, cost-effective, and not demanding complex equipment, they have gained interest in attaining porous PDMS foams [26]. The sacrificial templates are dispersed into the PDMS matrix during synthesis and are removed only after vulcanization, often by suitable solvents [25]. The pore morphologies of the porous PDMS foams are tuneable and reliant on the microstructure of the said templates. Household and inexpensive solid particles such as sugar, salt, citric acid monohydrate, or polystyrene beads have been used as sacrificial templates to fabricate porous PDMS structures [26–30]. These particles are impregnated into the precursor matrix and are later dissolved in solvents after curing, leaving behind a porous network, with ethanol and water being the most popular solvents of choice [18].

When an immiscible liquid template is used, the process is now termed emulsion templating, as a two-phase system is created [31]. The liquid is homogenized with the PDMS blend into droplets as the internal phase, and serves as templates for the resultant porous structures. The concentration of the internal phase leads to porous structures with tuneable morphologies [32]. After polymerization, the internal phase is either evaporated or solvent-extracted. For emulsion templating, water has been the most commonly used internal phase [20,33–35]. Solvents acting as the internal phase such as perfluorocarbon and hexane have been reported as well [22,36]. Alcohols such as methanol, ethanol, and propanol have been investigated [11].

The templated porous PDMS structures are typically fabricated via mould casting, which necessitates multiple stages and equipment. Nonetheless, fabrication with mould

casting often limits the structural flexibility and geometrical features of porous PDMS structures. Hence, three-dimensional (3D) printing has been implemented to allow for more intricate designs and geometries to broaden its applications [8]. There are a number of methods applied for printing silicone, such as material extrusion printing or direct ink writing (DIW), freeform reversible embedding, and vat photopolymerization [37]. DIW is famous for its ease of setup and operation, as well as high versatility with a breadth of compatible feedstock or inks [38]. The compatible inks for DIW consist of fine particles homogeneously dispersed in a liquid medium and behaving like a solid, also commonly known as gel. Essentially, inks are continuously extruded and flow through a nozzle to form a continuous filament which is then stacked in a layered manner to fabricate a printed article [39].

There are numerous cases of DIW of PDMS-based inks. To implement DIW, these inks must fulfil specific rheological features. In short, the inks should be viscoelastic with adequate yield stress to resist deformation for layer stacking, as well as exhibiting shear-thinning characteristics to enable smooth extrusion through the nozzle [40]. Besides these, the storage modulus of such inks must be high for shape retention at low shear-stresses to manifest a solid-like nature [21]. In contrast, inks with low storage modulus and insufficient yield stress will slump under their own mass, while inks with high viscosities might not be extrudable via small nozzle diameters, with such cases ultimately leading to print failure [40–42]. However, researchers have achieved the desired printing rheology for PDMS-based inks, either by blending PDMS components of different viscosities, incorporating fillers as rheology modifiers, or by speeding up curing of low viscosity inks with precuring treatments during printing [43].

By incorporating templated inks with porogens and DIW printing techniques, one is able to integrate intrastrand porosity in the extruded filaments to build hierarchically porous constructs, leading to a greater degree of tunability of mechanical properties [44,45]. When solid particles are used for templating, printing is limited by the nozzle diameter. When large particles or agglomerates are paired to a small nozzle diameter, there is a risk of the nozzle clogging during printing. For instance, Adhikari et al. [46] had to grind salt particles into smaller sizes prior to mixing with PDMS precursor to reduce the risk of the nozzle clogging when printing. The PDMS precursor in liquid form was homogeneously mixed with the ground salt particles and subsequently used as the printing ink for an extrusion-based printer. The formulated ink was able to conform to the diameter and geometry of the nozzle's tip, for successful printing [34].

Herein, porous PDMS foams were constructed via emulsion templating. Samples were printed via DIW. Glycerol as the internal phase was distributed into a one-part room-temperature vulcanizing (RTV-1) silicone formulation via high-speed centrifugal mixing, prompting stable glycerol/PDMS emulsions. After vulcanization, samples were immersed into ethanol to remove glycerol, eventually producing porous foams. The glycerol amounts in these inks were varied to study the effects of glycerol dosage on a few dependent silicone properties, including the rheological properties of the silicone ink, the pore properties, and subsequent tensile and compressive properties. Through the characterization studies and results obtained, few empirical models were derived that defined the correlation between the dispersed glycerol phase and the foam's pores properties and mechanical properties well. In addition, these models facilitate the customization of future silicone foams with varying pore and mechanical properties. Finally, a simple piezoresistive sensor was fabricated to showcase the potential application of the templated PDMS/glycerol foam.

2. Materials and Methods

2.1. Materials

The base polymer of choice was α,ω-silanol-terminated polydimethylsiloxane (PDMS), with a viscosity of 20,000 CPs. Methyl tris (methyl ethyl ketoxime) silane crosslinker was utilized. Fumed nanosilica filler with a BET surface area of 100 m^2/g and average primary particle size of 5–40 nm was used as purchased to bring forth shear-thinning characteristics. All chemicals were used as purchased from SiSiB® Silicones Co., Ltd., Nanjing, China. Analytical-grade glycerol was used as purchased from Merck KGaA, Darmstadt, Germany, to create glycerol/PDMS silicone ink emulsions. Absolute ethanol was used as purchased from Merck for solvent extraction to produce porous PDMS samples. Conductive carbon black was used as purchased from Suzhou Sinero Technology Co., Ltd., Suzhou, China.

2.2. PDMS Foam Preparation

To create stable emulsions, a planetary mixer (Kakuhunter SK300SII from Shashin Kagaku Co., Ltd., Kusatsu, Japan) was utilized in a manner similar to a previous work [47]. Firstly, the polymer blend was speed-mixed and degassed with glycerol at 2000 rpm for 30 s. The high-shear forces induced by the mixer conceived stable emulsions without the aid of any surfactants. Next, nanosilica was added and manually mixed before undergoing an identical speed-mixing and degassing sequence. Five ink formulations with glycerol contents of 10, 20, 30, 40, and 50 parts per hundred rubber (phr) and appropriate nanosilica content for printable structures were studied and listed in Table 1. With respect to the different glycerol concentrations used, the appropriate nanosilica concentration was identified to satisfy the rheological requirements for DIW. The mass of each chemical used for the inks is listed in Table S1. DIW of the samples was carried out via a lead screw-based extrusion printer. Print parameters were kept at a speed of 10 $mm \cdot s^{-1}$, via a nozzle of 0.84 mm diameter and a layer height of 0.4 mm. Samples were printed with 100% infill density to ensure porosity was entirely due to leaching of glycerol through solvent extraction. The dimensions of all samples are listed in Table S2.

Table 1. Ink formulations for printable silicone foams.

Ink Designations	Glycerol (phr)	Nanosilica (phr)	PDMS (phr)	Crosslinker (phr)
I1	10	8	100	16.23
I2	20	10	100	16.23
I3	30	12	100	16.23
I4	40	14	100	16.23
I5	50	14	100	16.23

2.3. Solvent Extraction for Porous PDMS Samples

To create porous PDMS samples, the liquid glycerol entrapped in printed silicone elastomer structures was extracted by immersion in ethanol. All prepared silicone samples were printed immediately after ink preparation and left to be cured in ambient conditions for at least 48 h before solvent extraction was performed to promote consistent results. For the solvent extraction process, samples were immersed and stirred in analytical-grade ethanol for 24 h at room temperature, followed by oven drying at 60 °C until constant mass was achieved.

2.4. Rheology Characterization

The rheological behaviour of all ink formulations was characterized using a Physica MCR 301 rheometer from Anton Paar GmbH, Graz, Austria. All experiments were con-

ducted using a 25 mm diameter parallel plate fixture geometry with a working gap of 1 mm. Flow curves or the viscosity of the inks were studied with shear rate ranging from 0.1 s^{-1} to 100 s^{-1}. Amplitude sweeps with angular frequency of 10 rad·s^{-1} and shear strain ranging from 0.01% to 100% were performed to gauge the linearity limit of the linear viscoelastic region (LVR) of different silicone ink formulations. The linearity limit was selected as the point where the storage modulus (G′) deviated 10% from the plateau, in accordance with the ASTM D7175 standard [48]. The yield stress was the corresponding shear stress value at the said limit. The stability of the silicone ink formulations, storage modulus (G′), loss modulus (G″), and loss factor (tan δ) were verified from frequency sweep tests, ranging from 0.1 rad·s^{-1} to 100 rad·s^{-1} at an amplitude of 0.01% shear strain. All tests were carried out in triplicate and at ambient temperature.

2.5. Porosity Characterization

The internal pore morphology of porous PDMS samples was illustrated via scanning electron microscopy (SEM) with the Hitachi S-3400N model from Hitachi High-Technologies Corporation, Tokyo, Japan. The samples were rapidly frozen in liquid nitrogen solution for 5 min, followed by cutting of the samples axially with a knife to expose and image the cross-sectional area of all foam samples. The probe current and acceleration voltage were set at 20 mA and 15kV, respectively. All samples were coated with a layer of palladium and gold prior to imaging. ImageJ (version 1.54d) image analyser was employed to statistically characterize the average pore size, pore size distribution, and pore area, similar to previous studies [20,49]. At least 5 SEM images for each sample were analysed, with the sample size of more than 150 pores. The porosity of each sample was then calculated with Equation (1), below:

$$\text{Porosity} = (\Sigma \text{ Pore area in an image})/(\text{Image Area}). \quad (1)$$

2.6. Mechanical Characterization

The tensile properties of porous PDMS samples were assessed in compliance with ASTM D412 standards [50], with the type-C "dog bone" geometry [51,52]. The compressive properties were then investigated via ASTM D575-91 standards [53], with test samples measuring 12.9 mm and 29 mm in thickness and diameter respectively [54,55]. Both sets of tests were implemented using a AGS-100 kNX universal testing machine from Shimadzu Corporation, Kyoto, Japan. Multiple samples were 3D printed based on the type-C "dog bone" geometry and cylinders with dimensions of 12.9 mm thickness and 29 mm diameter for tensile and compression tests, respectively. The mechanical testing for the printed samples was run in triplicate and the average readings of both tensile and compression tests are reported here.

2.7. Piezoresistive Effect

A porous silicone scaffold with a 50% infill was printed based on a 3D CAD model with dimensions of 25 mm × 25 mm × 10 mm. The scaffold was dip-coated in an ethanol/conductive carbon black solution and ultrasonicated. After drying, the strain sensor was fabricated. The resistance values of the silicone foam-based strain sensor were measured with a CD800a digital multimeter from Sanwa Electric Instrument Co., Ltd., Higashiosaka, Japan. The sensitivity of the sensor was measured using the AGS-100 kNX universal testing machine from Shimadzu Corporation, Kyoto, Japan where the sensor sample was subjected to compression strain values of 10%, 30%, 50%, and 70%. The corresponding resistance values were reported to exhibit the relationship between mechanical strain and the resistivity of the sensor.

3. Results and Discussion

3.1. Rheology

For DIW to work, it is vital for inks to achieve particular rheological properties. It is said that inks should be viscoelastic in nature with ample yield strength for shape retention after deposition through the printing nozzle, as well as possessing shear-dependent flow behaviour that facilitates extrusion at sensible pressures [40]. To ensure successful printing, the instantaneous rheological behaviour at the time of printing is important to ensure the fidelity of the 3D printed structure, while the rheological behaviour of the ink after printing varies mildly with time (viscosity and static yield stress mildly increase with time) due to the slow curing process which requires two days for complete curing. Thus, the continuous hardening of the deposited ink due to the curing process further maintains the rigidity of the structure. The rheological properties of interest that describe the glycerol/PDMS silicone inks used are summarised in Table 2 with a percentage error of ±5%. The viscosity values of the ink formulations were compared at the estimated shear rate $\dot{\gamma}$ experienced by the inks during printing via Equation (2) [40]:

$$\dot{\gamma} = (4\dot{Q})/(\pi r^3). \quad (2)$$

with r as the nozzle radius and $\dot{Q} = Sr^2$ as the volumetric flow rate, and where S denotes the printing speed. Hence, with a printing speed of 10 mm·s^{-1} and nozzle radius of 0.42 mm used, the inks are subjected to an approximate shear rate of 30.32 s^{-1}.

Table 2. Rheological properties of ink formulations used.

Ink Formulation	Static Yield Stress, σ_y^{Stat} (Pa)	Dynamic Yield Stress, σ_y^{Dyn} (Pa)	Viscosity (Pa·s)	Storage Modulus, G'_{LVR} (Pa)
I1	341.01	100.50	60.66	6461.94
I2	318.83	191.00	55.73	8187.86
I3	346.32	221.60	60.84	9286.62
I4	338.63	249.70	72.36	9451.39
I5	318.47	185.20	47.43	6677.00

Figure 1a presents the storage (G′) and loss (G″) moduli of the viscoelastic inks. All ink formulations initially exhibited solid-like behaviour (G′ > G″) along the linear viscoelastic region (LVR) and the inks flowed in a liquid manner after the crossover points (G″ > G′), where loss moduli were larger than storage moduli. With increasing shear stress, the values of G′ were consistent (plateau-like) up to the LVR limit, which can be termed as G'_{LVR}. After this limit, a further increase in shear stress led to the drop of G′ from the plateau. It is asserted that after this point, structural breakdown of the material had occurred, which led to permanent deformation, with the shear stress at the LVR limit corresponding to the static yield stress of the sample, while G'_{LVR} values are said to characterize the structural stiffness of an ink at rest [56]. Xu et al. [57] and Tang et al. [58] stated that the PDMS ink used for DIW had G′ values of 1×10^3 Pa and above. The ink formulations used in the current study had G′ values ranging from 6×10^3 Pa to 9×10^3 Pa, which implied that all formulated inks possessed adequate yield stress to maintain the structural integrity of the printed object using the DIW technique.

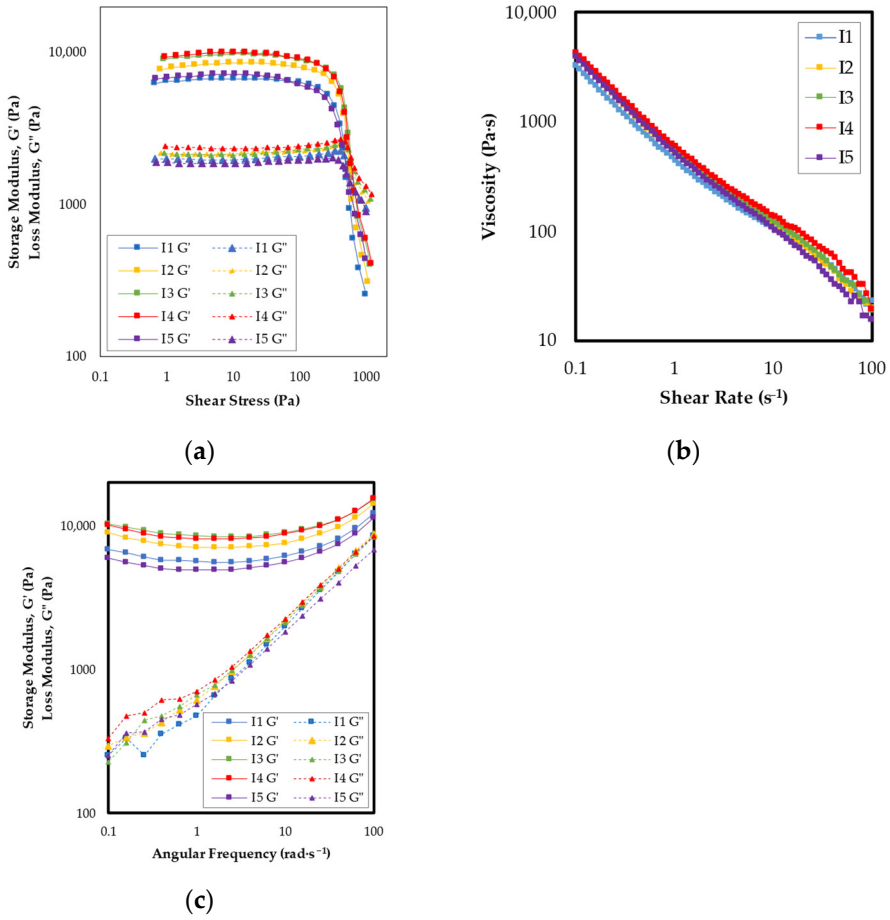

Figure 1. Rheological tests of inks used: (**a**) amplitude sweeps; (**b**) flow curves; (**c**) frequency sweeps.

The flow curves in Figure 1b illustrate that all inks exhibited shear-thinning flow behaviour, portrayed by the drop in viscosities with increasing shear rates, allowing the extrusion of highly viscous inks. The inks used in this study demonstrated relatively low viscosities of 47.43 Pa·s to 60.66 Pa·s at a shear rate 30.32 s^{-1}, as smooth extrusion was achieved from the lead-screw extrusion system. The yield stresses of viscoelastic inks are crucial for successful printing. It was theorized that the static yield stress ${\sigma_y}^{Stat}$ implies the minimum stress required that a fluid must overcome to initiate flow from rest, while the dynamic yield stress ${\sigma_y}^{Dyn}$ signifies the stress required for the fluid in motion to maintain flow [40]. A larger ${\sigma_y}^{Stat}$ is desired for the ink to be self-sustaining and possess solid-like behaviour, while the ${\sigma_y}^{Dyn}$ has to be higher than the shear stress applied during printing to withstand deformation of stacking layers [40,51]. As shown in Table 2, all ink formulations used revealed ${\sigma_y}^{Stat}$ values exceeding 300 Pa, which led to good shape fidelity. The yield stress values agreed with the study conducted by Courtial et al. [59], in which their static yield stress values exceeded 300 Pa and were sufficient for extrusion-based printing of silicone elastomer, while Lyu et al. [60] reported printable static yield stress values between 10^2 to 10^3 Pa. The dynamic yield stress ${\sigma_y}^{Dyn}$ of the thixotropic inks was obtained by curve-fitting the flow curves in Figure 1b with the Herschel–Bulkley model, as shown in Equation (3) [40,61]:

$$\sigma = \eta\dot{\gamma} = {\sigma_y}^{Dyn} + k\dot{\gamma}^{n} \quad (3)$$

where σ is the applied shear stress, η is the apparent viscosity, k is the consistency factor, $\dot{\gamma}$ is the shear rate, and n is the flow index. The ${\sigma_y}^{Dyn}$ values of all inks ranged from 100 Pa to 200 Pa and above, which is beyond the minimum value of 100 Pa reported by Danner et al. [62] for printable PDMS inks.

The frequency sweeps in Figure 1c serve as the curve function of the loss factor, also known as tan δ, of the inks across a range of angular frequencies. The loss factor is the ratio of loss to storage moduli of the inks (G''/G'), which indicates that the ink behaves as an elastic solid (tan $\delta < 1$) or viscous liquid (tan $\delta > 1$) [63]. The results established that no cross-over points (tan $\delta = 1$) were recorded for any ink formulations. The inks were solid-like as G' dominated G'' (tan $\delta < 1$) even at high angular frequencies and thus the inks are suitable for DIW printing [51,64].

3.2. Porosity

The printed glycerol/PDMS samples were left to cure in ambient conditions for at least 48 h, as shown in Figure 2. All samples were printed with the same print settings and geometry with no observable difference between the different ink formulations. Solvent extraction was then performed by immersing samples into ethanol to leach out glycerol droplets from the bulk material, leaving behind silicone foam with porous structures. The morphologies of all silicone foams depicted by the SEM images in Figure 3 demonstrated the effectiveness of the emulsion templating process in creating highly porous structures. Overall, spheroidal pores with distinct pore sizes and degrees of porosity were identified with responses to the different ink formulations employed. When more glycerol was present, the number of pores was more distinct, with enlarged pore sizes. This evidenced that tuneable pore properties were achievable by altering the glycerol content of the ink formulations, similar to the study by Chen et al. [65], which noted that pore size and porosity had increased due to higher loading of the sacrificial template introduced in their inks Glycerol as the dispersed phase in the silicone emulsion was responsible for the pore formation in the silicone structures. The pores formed by the glycerol droplets in the glycerol/PDMS emulsion were spheroidal in nature as the glycerol/PDMS interface tends to achieve minimum surface energy [8]. The pore size distributions and pore properties with respect to the different ink formulations are shown in Figure 4 and Table 3, respectively.

Table 3. Pore properties of ink formulations used.

Foam Samples	D10 (μm)	D50 (μm)	D90 (μm)	Standard Deviation (μm)	Average Pore Diameter (μm)	Porosity (%)
I1	1.00	1.78	3.22	0.97	2.02	7.16
I2	1.44	2.44	4.22	1.19	2.71	11.91
I3	1.56	2.89	5.40	1.97	3.31	22.77
I4	1.70	4.10	7.90	2.52	4.61	25.80
I5	2.00	3.90	8.10	2.75	4.66	27.63

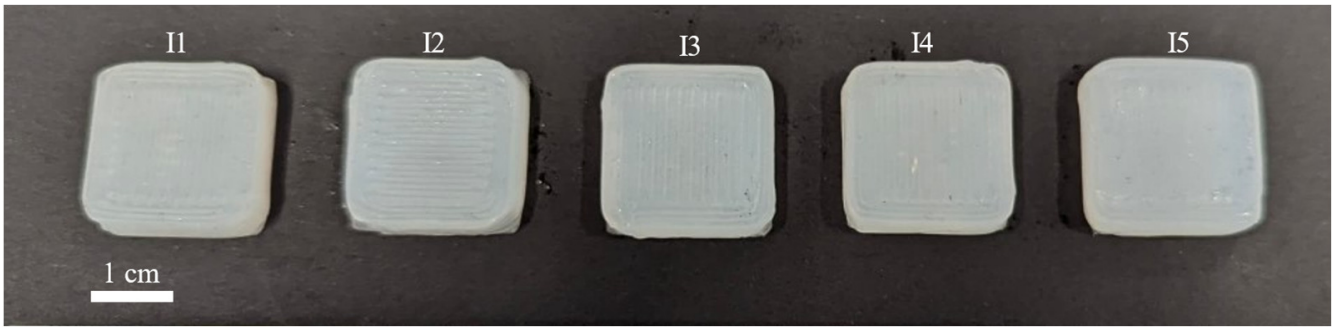

Figure 2. Printed samples of I1 to I5 from left to right.

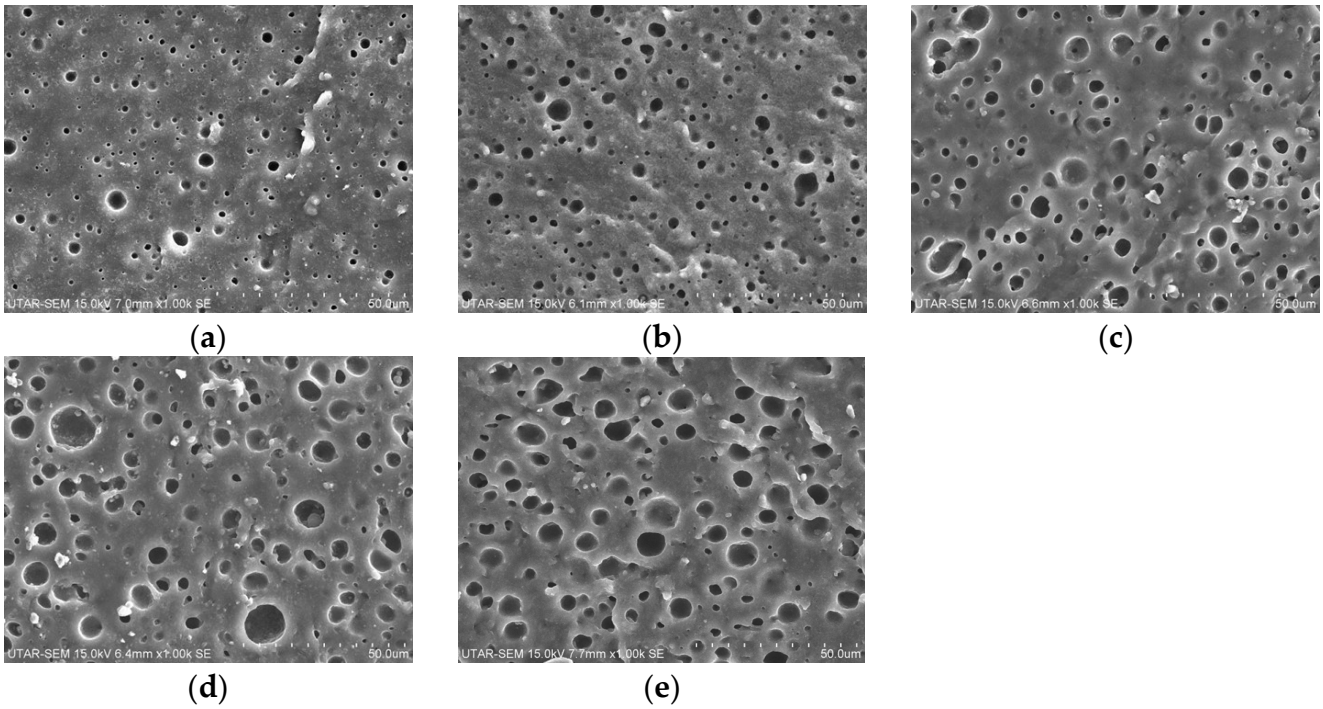

Figure 3. SEM images of foam samples: (**a**) I1; (**b**) I2; (**c**) I3; (**d**) I4; and (**e**) I5. Red arrows indicate the presence of pores in foam samples.

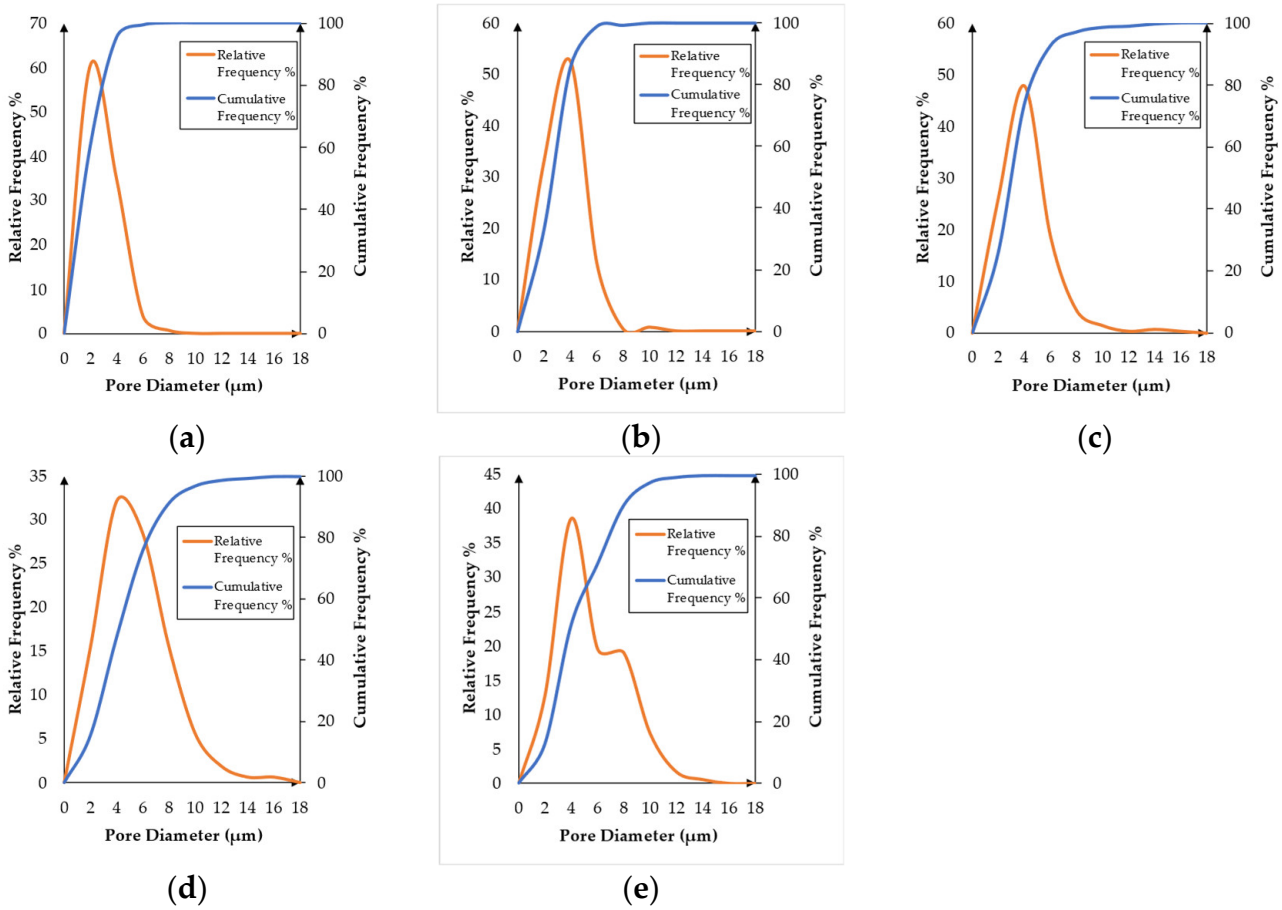

Figure 4. Pore size distributions of foam samples for (**a**) I1; (**b**) I2; (**c**) I3; (**d**) I4; and (**e**) I5.

Based on the data shown in Table 3, all foam samples were categorized as macropores [10], as the pore diameters ranged from 2.02 μm to 4.66 μm. For instance, in their work with water as the dispersed phase followed by droplet evaporation to create the foam structure, Kwak et al. [35] reported an average pore diameter of less than 3 μm when 5 wt% water was used, while in the work reported by Turco et al. [11], the pore sizes ranged from 1.768 μm to 65.8 μm with 50 wt% water. Thus, the pores sizes formed in the current study are comparable with other polymeric foams. In addition, the porosities varied from 7.16% to 27.63%, with 20.47% increments when the glycerol content increased from 10 phr to 50 phr. This implied that the silicone foam porosities are tuneable by manipulating the glycerol content alone. In fact, the porosity of the silicone foam was higher than the values declared by Abshirini et al. [20], where their emulsion system consisted of 20 vol% water and various surfactants had porosities between 15% and 25%.

The correlations between glycerol content and each of the abovementioned properties were curve-fitted using Matlab (R2022a) to the linear regression model, and the empirical models generated are listed in Equations (4)–(6) below, showing high goodness of fit, R^2. The level of distribution of pore diameter formed (indicated by standard deviation value), average pore diameter, and porosity of the silicone foam are linearly proportional with glycerol concentration in the glycerol/PDMS ink formulations as shown in Figures 5–7, respectively. The increment of average pore diameter, standard deviation, and porosity with increased glycerol concentration could be caused by the Ostwald ripening phenomenon. The Ostwald ripening phenomenon explained that the small sol particles are first dissolved and then redeposited onto larger sol particles in liquid sol, such as glycerol droplets in silicone emulsion. The tendency of small sol particles is to redeposit onto larger sol particles to form different pore diameters, despite the average pore diameter increasing with glycerol concentration.

$$y_1 = 0.1005\, x_1 \quad (4)$$

where y_1 represents glycerol content (vol%) and x_1 is the standard deviation of pore sizes (μm), with R^2 of 0.9799.

$$y_2 = 0.1804\, x_2 \quad (5)$$

where y_2 represents glycerol content (vol%) and x_2 is the average pore diameter (μm), with R^2 of 0.9481.

$$y_3 = 1.034\, x_3 \quad (6)$$

where y_3 represents glycerol content (vol%) and x_3 is the porosity (%), with R^2 of 0.9717.

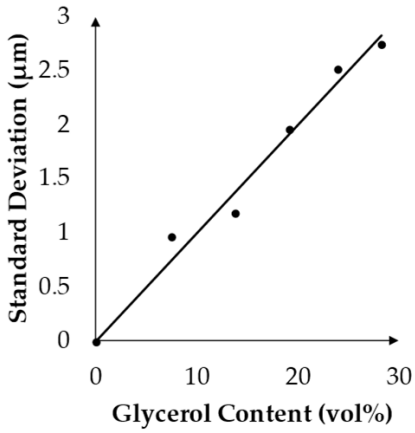

Figure 5. Relationship between glycerol content and standard deviation of pore sizes.

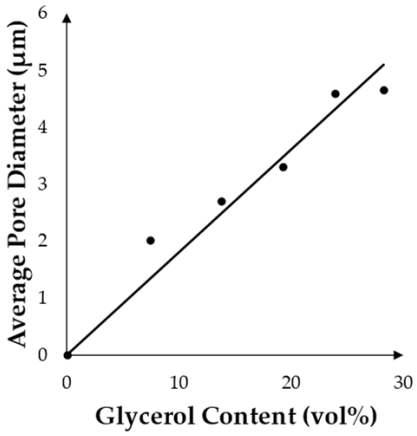

Figure 6. Relationship between glycerol content and average pore diameter.

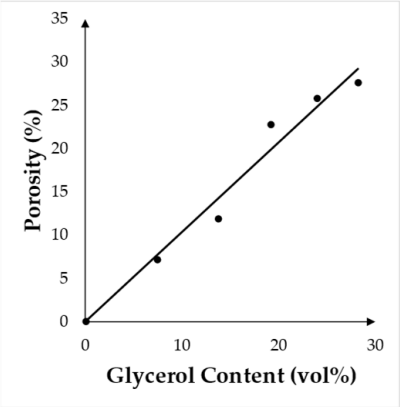

Figure 7. Relationship between glycerol content and porosity.

From Equations (4) and (5), the linear coefficients of standard deviation (0.1005) and pore diameter (0.1804) to the glycerol content were low, indicating that the remarkable increment in glycerol content only led to little increment in standard deviation of pore and pore diameter. However, an almost similar proportion of porosity can be achieved with respect to the glycerol concentration used, as revealed by its linear coefficient value of 1.034 from Equation (6). The linear correlation between glycerol concentration and the standard deviation of pore sizes, average pore diameter, and porosity verified that the tuneability of pore properties is achievable under the emulsion templating process. Glycerol droplets acted as the internal phase and were successfully leached out by ethanol, leaving behind a porous structure in the bulk PDMS continuous phase. The immiscible glycerol droplets were effectively dispersed within the PDMS blend prior to vulcanization due to the high shear forces induced during centrifugal mixing [66]. All glycerol/PDMS ink formulations used can be classified under low internal phase emulsion (LIPE), as the silicone formulations have an internal phase lower than 30 vol%, while polymerized samples after curing are termed polyLIPEs [20]. In the current study, the glycerol/PDMS emulsions were stable with glycerol concentrations between 7.46 vol% and 28.22 vol%, while phase separation was observed beyond 28.22 vol%, as it was assumed that the maximum packing density of glycerol in the current PDMS blend had been reached. The enlargement of average pore diameter, standard deviation, and porosity can be associated with the Ostwald ripening phenomenon [67]. Furthermore, it was theorized that the glycerol/PDMS inks were stabilized by nanosilica particles prior to vulcanization, without the presence of any surfactants or emulsifiers. Such emulsions are named Pickering emulsions [68]. The nanosilica particles had formed a physical barrier between the glycerol droplets and the

PDMS matrix, which "locked-in" the internal phase to prevent excessive droplet coalescence and inhibiting further Ostwald ripening [20]. Essentially, the immiscible glycerol and the PDMS blend were combined into a stable emulsion through high mechanical forces via centrifugal mixing without the need of surfactants, while silica nanoparticles confined the droplets in place, allowing for printing and subsequent vulcanization of samples.

3.3. Tensile Properties

Figure 8a shows the stress–strain curves for foam samples with varying porosity. The foam samples displayed excellent elastic and ductile behaviours, as the increase in stress (0.68–0.93 MPa) resulted in 670–750% of elongation compared to the original length [69]. All curves experienced an enormous elastic region, followed by a tiny plastic region where the samples could maintain their elasticity properties and reversibly return to their original shape though under wide range of stress, 0.6 MPa to 0.9 MPa. In the elastic region, the samples' stress initially rose linearly with strain followed by nonlinearity of strain increment up to the elasticity limit [70].

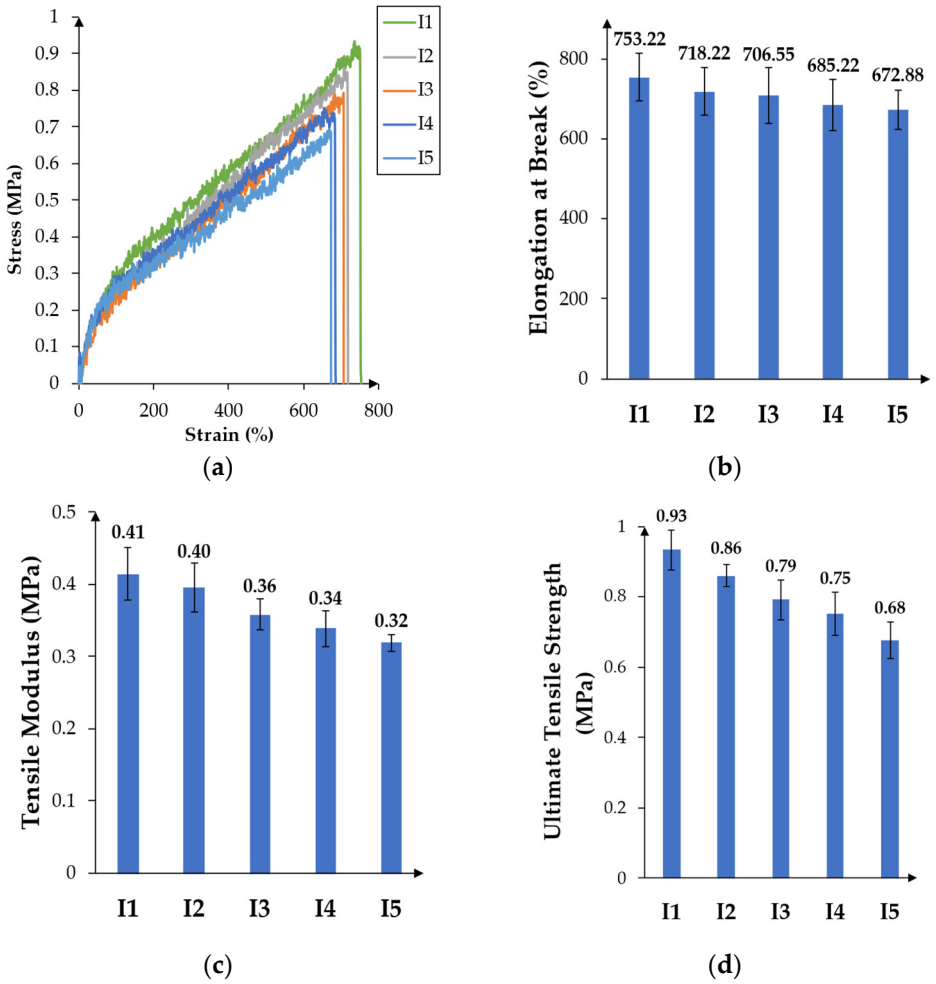

Figure 8. Tensile testing and the properties of glycerol/PDMS foam samples. (**a**) Stress–strain curves; (**b**) elongation at break; (**c**) tensile modulus; and (**d**) ultimate tensile strength.

From Figure 8b–d, the elongation at break, tensile modulus, and ultimate tensile strengths of all foams illustrated a downwards trend with the increment in glycerol concentration used in the ink formulation from I1 to I5. With increasing porosity due to the increasing glycerol concentration used, the tensile modulus dropped from 0.41 MPa to 0.32 MPa, while the ultimate tensile strength decreased from 0.93 MPa to 0.68 MPa. Judging

by the tensile modulus, the foams in this work were up to 81% less stiff than a similar 3D-printable nonporous silicone ink prepared by Lim et al. [63], which had a modulus of 1.69 MPa. This signifies that introducing porosity to the silicone sample can effectively reduce the stiffness of the printed silicone samples. Moreover, all silicone foams resulting from varied ink formulation (I1 to I5) possessed outstanding ductility, with elongation at break values stretching from 672.88% to 753.22%. The 20.47% increase in porosity from I1 and I5 decreased the elongation at break, tensile modulus, and ultimate tensile strength of the foam samples by 10.67%, 21.95%, and 26.88%, respectively. This denotes that the glycerol content in the glycerol/PDMS ink formulations and subsequent porosity could alter the mechanical properties, especially the ultimate strength of the PDMS foams, the most.

Figures 9–11 correlate the relationship between porosity and the tensile modulus, ultimate tensile strength, and elongation at break respectively. The data fitted well to the linear regression models, as indicated by high R^2 values of 0.98–0.99. The tensile modulus, ultimate tensile strength, and elongation at break were inversely proportion to the porosity, as indicated in Equations (7)–(9).

$$y_4 = -0.0048\, x_4 + 0.4537 \quad (7)$$

where y_4 represents porosity (%) and x_4 is the tensile modulus (MPa), with R^2 of 0.9853.

$$y_5 = -0.012\, x_5 + 1.025 \quad (8)$$

where y_5 represents porosity (%) and x_5 is the ultimate tensile strength (MPa), with R^2 of 0.9929.

$$y_6 = -3.773\, x_6 + 777.1 \quad (9)$$

where y_6 represents porosity (%) and x_6 is the elongation at break (%), with R^2 of 0.9803.

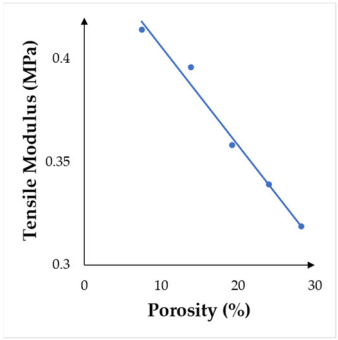

Figure 9. Relationship between porosity and tensile modulus. The solid line shows an empirical model fitted to the data.

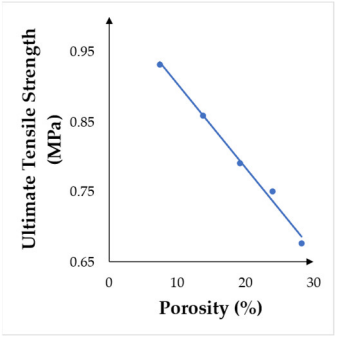

Figure 10. Relationship between porosity and ultimate tensile strength. The solid line shows an empirical model fitted to the data.

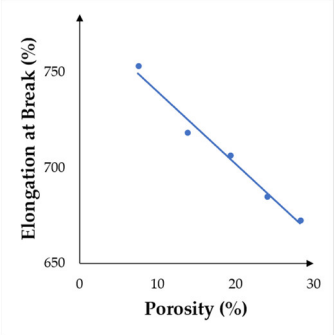

Figure 11. Relationship between porosity and elongation at break. The solid line shows an empirical model fitted to the data.

The tensile modulus, ultimate tensile strength, and elongation at break of a material were declared to be negatively influenced by porosity [71–73]. In this study, the glycerol introduced into the glycerol/PDMS inks had largely reduced the matrix fraction. The foams produced after solvent extraction had leached out the glycerol droplets, thus leaving voids in the PDMS matrix. The increase in macroporosity had diminished the numbers of bonding between the silicone backbone with crosslinkers and nanosilica, consequently reducing the effective volume of PDMS responsible for load bearing, as well as compromising crack propagation distance, leading to a drop in tensile characteristics [65]. It was also alleged that the increased number of voids led to more stress concentration points, leading to a weaker material [74]. Hence, it is conceived that a larger degree of porosity brings forth foams with lower tensile properties.

3.4. Compressive Properties

Figure 12a depicts the stress–strain response of foam samples under compression tests. Compression stress–strain curves for silicone rubber generally feature an initial linear region which associates with the foam's elastic behaviour, followed by a plateau region in which the strain is barely affected by increased stress due to the yielding and energy absorption of cell structures, and lastly the densification region, outlined by the sharp increase of the stress–strain slope due to the immense collapse of cell structures [73,75]. As in the tensile tests performed, foams with different porosity displayed different behaviour under compression testing. It is noticed that the plateau region was elongated in foams with higher porosity, suggesting that more closed cells were subjected to compression with higher energy absorption [44]. Larger pores necessitate a higher strain to achieve compression and filling of voids in the structure [63]. To inspect the compressive performance of all foams, one can contrast the corresponding compressive stress values at a fixed strain [73]. Hence, the compressive stress values at 80% strain of all samples were chosen for the comparison. Figure 12b,c conveys that the compressive modulus and compressive stress of foam samples from I1 to I5 lowered from 1.51 MPa to 0.94 MPa, as well as 10.08 MPa to 6.53 MPa, respectively. As a comparison, the compressive modulus of a commercialized room-temperature vulcanized silicone rubber is disclosed by Kumar et al. [76] as 1.55 MPa. Hence, the compressive modulus of the porous silicone foams synthesized in this study were comparable with commercial silicone rubber despite the compensation of moderate pore structures. The 20.47% greater degree of porosity from I1 to I5 prompted a reduction of 37.75% in compressive modulus, and 35.22% in compressive strength at 80% strain. In brief, the compressive properties of the foam samples were impacted and tuneable solely by the degree of porosity.

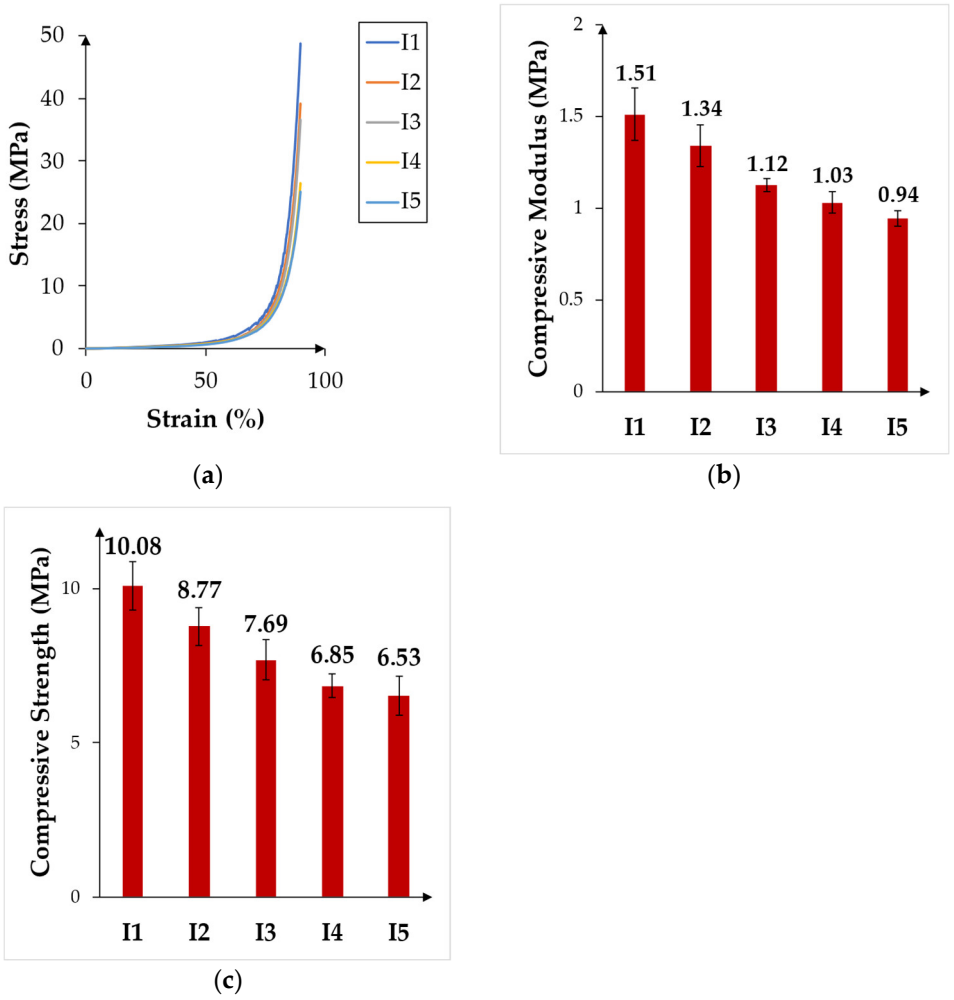

Figure 12. Compression testing and the properties of glycerol/PDMS foam samples. (**a**) Stress–strain curves; (**b**) compressive modulus; and (**c**) compressive strength.

Once again, the strong correlations between porosity and compressive modulus and compressive strength, respectively, as modelled by Equations (10) and (11), proved the inversely linear relationship between porosity and the foams' compressive properties in this study.

$$y_7 = -0.0256\, x_7 + 1.673, \quad (10)$$

Equation (10) fit the data well (Figure 13), where y_7 represents porosity (%) and x_7 is the compressive modulus (MPa), with R^2 of 0.9840.

$$y_8 = -0.1589\, x_8 + 11.01, \quad (11)$$

Equation (11) fit the data well (Figure 14), where y_8 represents porosity (%) and x_8 is the compressive strength at 80% strain (MPa), with R^2 of 0.9688.

Identical to the tensile tests, Figures 13 and 14 validate the descending trend of porosity on the foams' compressive modulus and compressive strength. The increase in porosity due to higher glycerol content had lessened the volume of PDMS and subsequently the numbers of covalent bonding responsible for load bearing during compression tests, thus resulting in the decreased compressive strength [77,78]. The lower compressive strength in samples was observed with larger pore sizes and porosity, which had been reported in the literature [79].

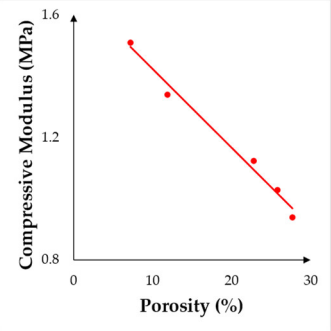

Figure 13. Relationship between porosity and compressive modulus. The solid line shows an empirical model fitted to the data.

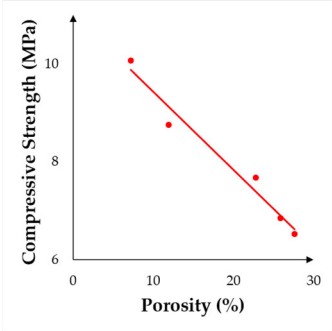

Figure 14. Relationship between porosity and compressive strength. The solid line shows an empirical model fitted to the data.

In comparison, the tensile strength and tensile modulus of all the porous silicone foams prepared under I1 to I5 were lower than the compressive strength and the compressive modulus. For instance, the tensile modulus of samples from I5 has a tensile modulus of 0.32 MPa, but its compressive modulus is 0.94 MPa. Obviously, the porous silicone foams with higher compressive strength were able to withstand heavy loads without deforming. In contrast, the silicone foams were prone to deforming or breaking when subjected to pulling and stretching, as indicated with lower tensile strength. This is as expected, as the tensile properties of silicone rubber are generally poorer than those of its compressive counterpart [80].

3.5. Potential Applications

All ink formulations satisfy the rheological properties required for DIW as reported in Table 2. Figure 15a illustrates a printed insole for medical applications. With DIW, insoles with tailor-made geometries can be printed to suit specific users. With varying porosity, insoles with different properties make it possible to fulfil different demands, from softer insoles or to stiffer insoles based on one's preference. Figure 15b,c demonstrates the printability of glycerol/PDMS inks with the successful printing of a Sierpinski pyramid and scaffold structure, respectively. Scaffolds with pore structures facilitates cell seeding and cell penetration throughout the entire scaffold to regenerate functionalized tissues and organs. These articles are complex and have intricate features, which demand inks with stringent viscoelastic behaviour. These denote that the yield stress and storage modulus of glycerol/PDMS inks were sufficient to retain shape fidelity and sustain layer stacking, as no slumping due to gravitational forces was detected. The viscosities of these inks were within the limit of the extrusion pressure generated by the leadscrew-based extrusion system used in this study, as the printed filaments were smoothly extruded to realize printed articles with accurate details.

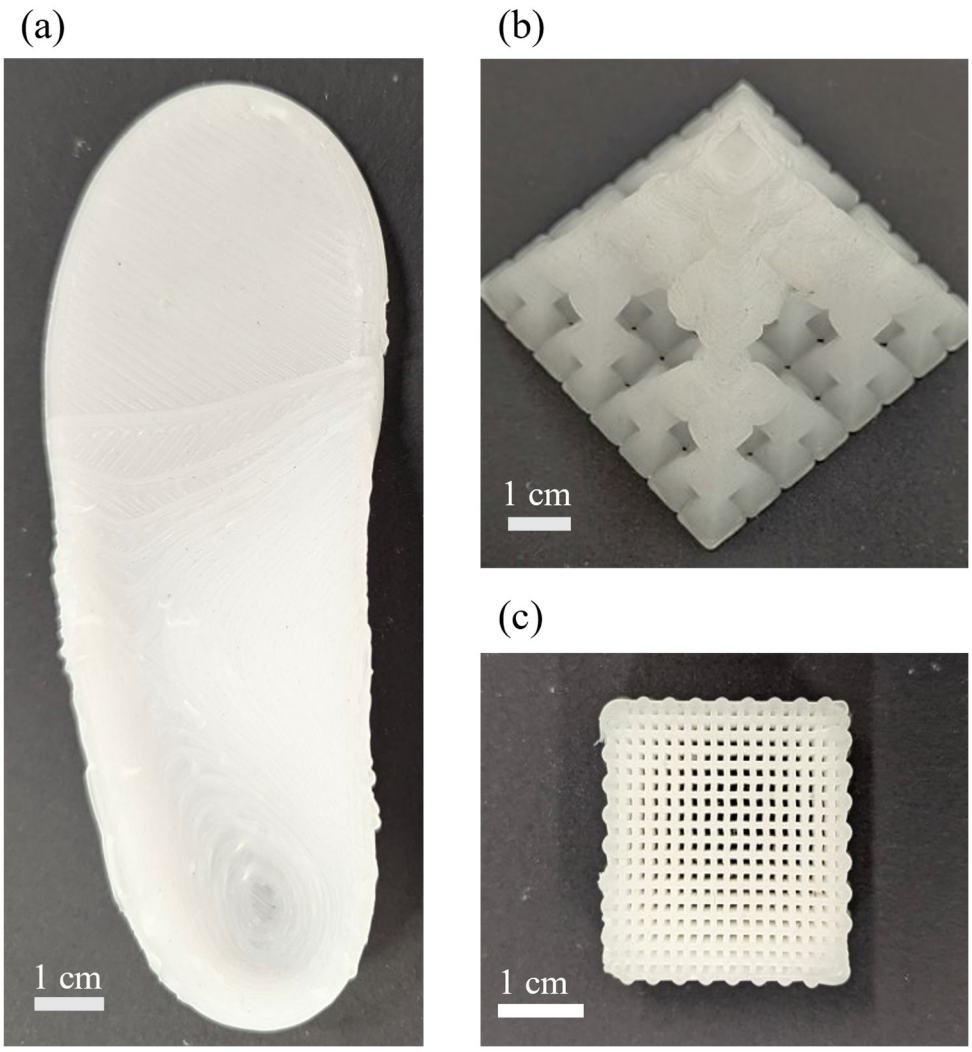

Figure 15. Printed articles: (**a**) insole; (**b**) Sierpinski pyramid; and (**c**) scaffold structure. All articles shown were printed with ink I5 and prior to glycerol extraction.

Another application for the emulsion-templated porous silicone foam was demonstrated to be a piezoresistive strain sensor. To fabricate the sensor, a printed scaffold structure was dip-coated in a solution of ethanol/conductive carbon black particles and dried, presented in Figure 16a. Measurements were recorded with the setup shown in Figure 16b, with the sensor sandwiched in between two copper electrodes and connected to a digital multimeter. The sensor was compressed using universal tensile testing at different strains and resistance values were recorded as shown in Figure 16c. The average electrical change of the piezoresistive sensor is evaluated as [21]:

$$\Delta R/R_0 = (R_0 - R_s)/R_{0,} \quad (12)$$

with R_0 and R_s as the resistance values without and with compression, respectively. The gauge factor GF is the slope of the graph of $\Delta R/R_0$ against strain.

Figure 17a records the deviation of resistance values when the sensor was subjected to different strains. It was apparent that the resistance of the sensor varied with different levels of stress applied. A linear-like relationship was perceived between resistance measured from the conductive silicone and the strain of the samples due to the stress applied. Furthermore, the slope of the linear range of relative resistance changes, also known as gauge factor, was equal to 1.3188 and it was considered to have high sensitivity. This

authenticates the piezoresistivity of the porous silicone scaffold, as the resistance of the conductive porous silicone scaffold increased almost linearly with the mechanical stress applied. At 10% strain, the $\Delta R/R_0$ value was 24.74%. Increasing up to 70% strain, a $\Delta R/R_0$ value of 86.67% was logged. As shown in Figure 17b, three cycles of compression and decompression at different arbitrary strains were carried out to simulate real-time monitoring of strain sensing. The arbitrary applied pressure was increased with each cycle, while the decompression rate was arbitrarily slower. Higher peaks were discovered when a larger force was applied. Hence, it is feasible to integrate the 3D-printable emulsion-templated porous silicone foams to detect human motion as wearable sensors.

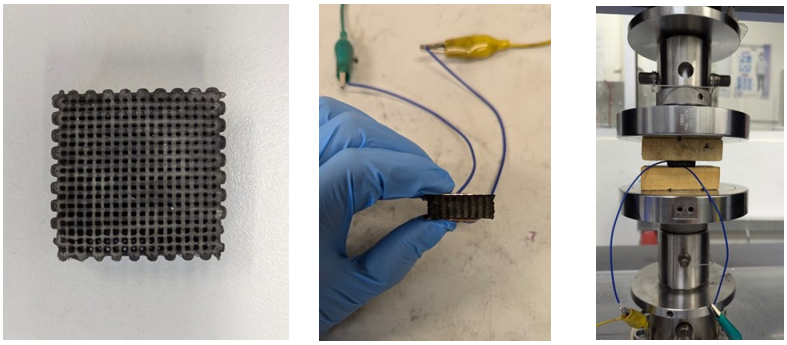

(**a**) (**b**) (**c**)

Figure 16. Strain-sensing application of porous silicone foam: (**a**) scaffold coated with carbon black; (**b**) setup for piezoresistive measurements; and (**c**) sensor under compression test.

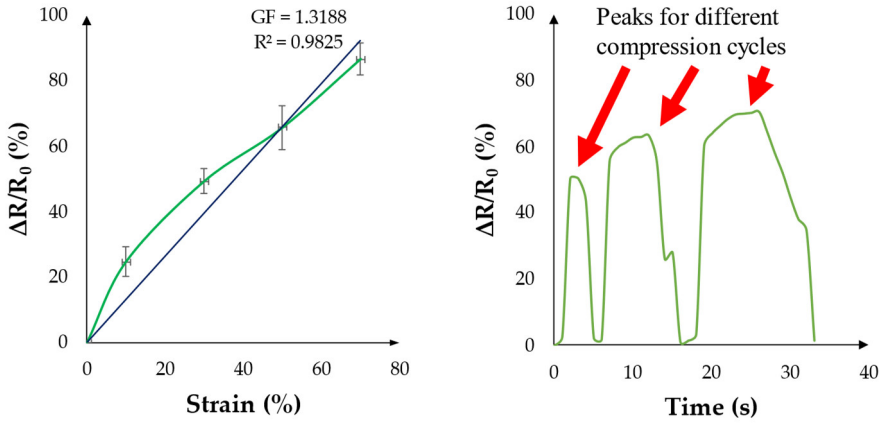

(**a**) (**b**)

Figure 17. Piezoresistive study of coated porous silicone scaffold: (**a**) resistance variation against compression strain; (**b**) simulation of strain sensing with different cycles of varying compression and decompression pressures and rates.

4. Conclusions

Porous silicone foams with tuneable properties were synthesized via a cost-effective and sustainable emulsion templating method. Three-dimensional printable ink emulsions with proper rheological properties for DIW were prepared by centrifugal mixing of a glycerol template into the PDMS precursor without requiring any surfactants. Porous silicone foams were obtained after solvent removal of glycerol. The pore properties and mechanical behaviour of the resultant foams were tuneable based on the glycerol content introduced as the sacrificial template. Based on the model derived, the pore properties were investigated to portray a linear relationship with the glycerol content. With every 10 phr increment of glycerol content in the ink formulations, the silicone foams' porosity

increased 10%, while the average pore diameter increased 2 µm. The foams with varying porosity mildly impacted the tensile properties, with every 10% porosity increment leading to slight drop of 0.07 MPa tensile strength and 0.02 MPa tensile modulus or stiffness. In contrast, the compressive strength experienced a decrement of 1 MPa for every 10% porosity increment. To demonstrate the functionality and printability of the 3D-printable porous PDMS inks, an insole and a conductive porous scaffold which acted as a piezoresistive strain sensor were printed successfully. The 3D-printed silicone foams with tuneable porosity, complex structures, and compatible mechanical strength and elasticity could accelerate the applications of silicone to diverse fields.

Supplementary Materials: The following supporting information can be downloaded at: https://www.mdpi.com/article/10.3390/pr13030677/s1, Table S1: Mass of chemicals used in glycerol/PDMS ink formulations; Table S2: Average sample dimensions.

Author Contributions: Conceptualization, K.W.T., J.H.S. and J.Y.T.; methodology, K.W.T., J.H.S., J.Y.T. and Z.H.L.; software, K.W.T. and J.H.S.; validation, W.H.Y., J.Y.T. and T.S.L.; investigation, K.W.T., J.H.S., J.Y.T. and Z.H.L.; resources, W.H.Y., L.Y.N., T.S.L. and L.C.A.; data curation, J.H.S., L.Y.N., S.T.B., T.S.L. and L.C.A.; writing—original draft preparation, K.W.T. and J.H.S.; writing—review and editing, K.W.T., J.H.S., L.Y.N., S.T.B. and L.C.A.; visualization, S.T.B., T.S.L. and L.C.A.; supervision, J.H.S., J.Y.T. and Z.H.L.; project administration, J.H.S., J.Y.T., W.H.Y. and Z.H.L.; funding acquisition, J.H.S., S.T.B. and T.S.L. All authors have read and agreed to the published version of the manuscript.

Funding: This research was supported by the Ministry of Higher Education (MoHE), through the Fundamental Research Grant Scheme (FRGS/1/2023/TK10/UTAR/02/1).

Data Availability Statement: The original contributions presented in this study are included in the article/Supplementary Materials. Further inquiries can be directed to the corresponding authors.

Conflicts of Interest: The authors declare no conflicts of interest.

Abbreviations

The following abbreviations are used in this manuscript:

PDMS	Polydimethylsiloxane
phr	Parts per hundred rubber
DIW	Direct ink writing

References

1. Si, J.; Cui, Z.; Xie, P.; Song, L.; Wang, Q.; Liu, Q.; Liu, C. Characterization of 3D Elastic Porous Polydimethylsiloxane (PDMS) Cell Scaffolds Fabricated by VARTM and Particle Leaching. *J. Appl. Polym. Sci.* **2016**, *133*, 1–9. [CrossRef]
2. Eduok, U.; Faye, O.; Szpunar, J. Recent Developments and Applications of Protective Silicone Coatings: A Review of PDMS Functional Materials. *Prog. Org. Coat.* **2017**, *111*, 124–163. [CrossRef]
3. Zare, M.; Ghomi, E.R.; Venkatraman, P.D.; Ramakrishna, S. Silicone-Based Biomaterials for Biomedical Applications: Antimicrobial Strategies and 3D Printing Technologies. *J. Appl. Polym. Sci.* **2021**, *138*, 50969. [CrossRef]
4. Owen, M.J. Silicone Surface Fundamentals. *Macromol. Rapid Commun.* **2021**, *42*, 1–9. [CrossRef]
5. Miranda, I.; Souza, A.; Sousa, P.; Ribeiro, J.; Castanheira, E.M.S.; Lima, R.; Minas, G. Properties and Applications of PDMS for Biomedical Engineering: A Review. *J. Funct. Biomater.* **2022**, *13*, 2. [CrossRef]
6. Ariati, R.; Sales, F.; Souza, A.; Lima, R.A.; Ribeiro, J. Polydimethylsiloxane Composites Characterization and Its Applications: A Review. *Polymers* **2021**, *13*, 4258. [CrossRef]
7. Kramer, S.; Krajnc, P. Hierarchically Porous Microspheres by Thiol-ene Photopoly-Merization of High Internal Phase Emulsions-in-water Colloi-Dal Systems. *Polymers* **2021**, *13*, 3366. [CrossRef]
8. Woo, R.; Chen, G.; Zhao, J.; Bae, J. Structure-Mechanical Property Relationships of 3D-Printed Porous Polydimethylsiloxane. *ACS Appl. Polym. Mater.* **2021**, *3*, 3496–3503. [CrossRef]
9. Berro, S.; El Ahdab, R.; Hajj Hassan, H.; Khachfe, H.M.; Hajj-Hassan, M. From Plastic to Silicone: The Novelties in Porous Polymer Fabrications. *J. Nanomater.* **2015**, *2015*, 142195. [CrossRef]

10. Pandey, K.; Bindra, H.S.; Paul, D.; Nayak, R. Smart Multi-Tasking PDMS Nanocomposite Sponges for Microbial and Oil Contamination Removal from Water. *J. Polym. Res.* **2020**, *27*, 189. [CrossRef]
11. Turco, A.; Primiceri, E.; Frigione, M.; Maruccio, G.; Malitesta, C. An Innovative, Fast and Facile Soft-Template Approach for the Fabrication of Porous PDMS for Oil-Water Separation. *J. Mater. Chem. A* **2017**, *5*, 23785–23793. [CrossRef]
12. Lv, J.; Gong, Z.; He, Z.; Yang, J.; Chen, Y.; Tang, C.; Liu, Y.; Fan, M.; Lau, W.M. 3D Printing of a Mechanically Durable Superhydrophobic Porous Membrane for Oil-Water Separation. *J. Mater. Chem. A* **2017**, *5*, 12435–12444. [CrossRef]
13. Zhang, A.; Chen, M.; Du, C.; Guo, H.; Bai, H.; Li, L. Poly(Dimethylsiloxane) Oil Absorbent with a Three-Dimensionally Interconnected Porous Structure and Swellable Skeleton. *ACS Appl. Mater. Interfaces* **2013**, *5*, 10201–10206. [CrossRef] [PubMed]
14. Razavi, M.; Primavera, R.; Vykunta, A.; Thakor, A.S. Materials Science & Engineering C Silicone-Based Bioscaffolds for Cellular Therapies. *Mater. Sci. Eng. C* **2021**, *119*, 111615. [CrossRef]
15. Díaz Lantada, A.; Alarcón Iniesta, H.; Pareja Sánchez, B.; García-Ruíz, J.P. Free-Form Rapid Prototyped Porous PDMS Scaffolds Incorporating Growth Factors Promote Chondrogenesis. *Adv. Mater. Sci. Eng.* **2014**, *2014*, 612976. [CrossRef]
16. Pedraza, E.; Brady, A.C.; Fraker, C.A.; Molano, R.D.; Sukert, S.; Berman, D.M.; Kenyon, N.S.; Pileggi, A.; Ricordi, C.; Stabler, C.L. Macroporous Three-Dimensional PDMS Scaffolds for Extrahepatic Islet Transplantation. *Cell Transplant.* **2013**, *22*, 1123–1125. [CrossRef]
17. Montazerian, H.; Mohamed, M.G.A.; Montazeri, M.M.; Kheiri, S.; Milani, A.S.; Kim, K.; Hoorfar, M. Permeability and Mechanical Properties of Gradient Porous PDMS Scaffolds Fabricated by 3D-Printed Sacrificial Templates Designed with Minimal Surfaces. *Acta Biomater.* **2019**, *96*, 149–160. [CrossRef]
18. González-Rivera, J.; Iglio, R.; Barillaro, G.; Duce, C.; Tinè, M.R. Structural and Thermoanalytical Characterization of 3D Porous PDMS Foam Materials: The Effect of Impurities Derived from a Sugar Templating Process. *Polymers* **2018**, *10*, 616. [CrossRef]
19. Masihi, S.; Panahi, M.; Maddipatla, D.; Hanson, A.J.; Bose, A.K.; Hajian, S.; Palaniappan, V.; Narakathu, B.B.; Bazuin, B.J.; Atashbar, M.Z. Highly Sensitive Porous PDMS-Based Capacitive Pressure Sensors Fabricated on Fabric Platform for Wearable Applications. *ACS Sens.* **2021**, *6*, 938–949. [CrossRef]
20. Abshirini, M.; Saha, M.C.; Cummings, L.; Robison, T. Synthesis and Characterization of Porous Polydimethylsiloxane Structures with Adjustable Porosity and Pore Morphology Using Emulsion Templating Technique. *Polym. Eng. Sci.* **2021**, *61*, 1943–1955. [CrossRef]
21. Abshirini, M.; Marashizadeh, P.; Saha, M.C.; Altan, M.C.; Liu, Y. Three-Dimensional Printed Highly Porous and Flexible Conductive Polymer Nanocomposites with Dual-Scale Porosity and Piezoresistive Sensing Functions. *Appl. Mater. Interfaces* **2023**, *15*, 14810–14825. [CrossRef] [PubMed]
22. Hwang, J.; Kim, Y.; Yang, H.; Oh, J.H. Fabrication of Hierarchically Porous Structured PDMS Composites and Their Application as a Flexible Capacitive Pressure Sensor. *Compos. Part B Eng.* **2021**, *211*, 108607. [CrossRef]
23. Davoodi, E.; Montazerian, H.; Haghniaz, R.; Rashidi, A.; Ahadian, S.; Sheikhi, A.; Chen, J.; Khademhosseini, A.; Milani, A.S.; Hoorfar, M.; et al. 3D-Printed Ultra-Robust Surface-Doped Porous Silicone Sensors for Wearable Biomonitoring. *ACS Nano* **2020**, *14*, 1520–1532. [CrossRef] [PubMed]
24. Kalkal, A.; Kumar, S.; Kumar, P.; Pradhan, R.; Willander, M.; Packirisamy, G.; Kumar, S.; Malhotra, B.D. Recent Advances in 3D Printing Technologies for Wearable (Bio)Sensors. *Addit. Manuf.* **2021**, *46*, 102088. [CrossRef]
25. Métivier, T.; Cassagnau, P. New Trends in Cellular Silicone: Innovations and Applications. *J. Cell. Plast.* **2019**, *55*, 151–200. [CrossRef]
26. Yu, C.; Yu, C.; Cui, L.; Song, Z.; Zhao, X.; Ma, Y.; Jiang, L. Facile Preparation of the Porous PDMS Oil-Absorbent for Oil/Water Separation. *Adv. Mater. Interfaces* **2017**, *4*, 1600862. [CrossRef]
27. Li, Q.; Duan, T.; Shao, J.; Yu, H. Fabrication Method for Structured Porous Polydimethylsiloxane (PDMS). *J. Mater. Sci.* **2018**, *53*, 11873–11882. [CrossRef]
28. Kang, S.; Lee, J.; Lee, S.; Kim, S.G.; Kim, J.K.; Algadi, H.; Al-Sayari, S.; Kim, D.E.; Kim, D.E.; Lee, T. Highly Sensitive Pressure Sensor Based on Bioinspired Porous Structure for Real-Time Tactile Sensing. *Adv. Electron. Mater.* **2016**, *2*, 1600356. [CrossRef]
29. Liu, J.; Han, Y.; Hua, W.; Wang, Y.; You, G.; Li, P.; Liao, F.; Zhao, L.; Ding, Y. Improved Flowing Behaviour and Gas Exchange of Stored Red Blood Cells by a Compound Porous Structure. *Artif. Cells Nanomed. Biotechnol.* **2019**, *47*, 1888–1897. [CrossRef]
30. Wang, Q.; Chen, A.; Gu, H.; Qin, G.; Zhang, J.; Xu, J.; Jiang, G.; Liu, W.; Zhang, Z.; Huang, H. Highly Interconnected Porous PDMS/CNTs Sandwich Sponges with Anti-Icing/Deicing Microstructured Surfaces. *J. Mater. Sci.* **2021**, *56*, 11723–11735. [CrossRef]
31. Zhang, T.; Sanguramath, R.A.; Israel, S.; Silverstein, M.S. Emulsion Templating: Porous Polymers and Beyond. *Macromolecules* **2019**, *52*, 5445–5479. [CrossRef]
32. Racles, C.; Bele, A.; Vasiliu, A.L.; Sacarescu, L. Emulsion Gels as Precursors for Porous Silicones and All-Polymer Composites—A Proof of Concept Based on Siloxane Stabilizers. *Gels* **2022**, *8*, 377. [CrossRef] [PubMed]

33. Riesco, R.; Boyer, L.; Blosse, S.; Lefebvre, P.M.; Assemat, P.; Leichle, T.; Accardo, A.; Malaquin, L. Water-in-PDMS Emulsion Templating of Highly Interconnected Porous Architectures for 3D Cell Culture. *ACS Appl. Mater. Interfaces* **2019**, *11*, 28631–28640. [CrossRef] [PubMed]
34. Rauzan, B.M.; Nelson, A.Z.; Lehman, S.E.; Ewoldt, R.H.; Nuzzo, R.G. Particle-Free Emulsions for 3D Printing Elastomers. *Adv. Funct. Mater.* **2018**, *28*, 1707032. [CrossRef]
35. Kwak, Y.; Jo, E.; Kang, Y.; Kim, J. Highly Transparent Porous Polydimethylsiloxane with Micro-Size Pores Using Water and Isopropanol Mixture. In Proceedings of the 2020 IEEE 33rd International Conference on Micro Electro Mechanical Systems (MEMS), Vancouver, BC, Canada, 18–22 January 2020; pp. 287–290.
36. Zhao, J.; Luo, G.; Wu, J.; Xia, H. Preparation of Microporous Silicone Rubber Membrane with Tunable Pore Size via Solvent Evaporation-Induced Phase Separation. *ACS Appl. Mater. Interfaces* **2013**, *5*, 2040–2046. [CrossRef]
37. Gharaie, S.; Zolfagharian, A.; Moghadam, A.A.A.; Shukur, N.; Bodaghi, M.; Mosadegh, B.; Kouzani, A. Direct 3D Printing of a Two-Part Silicone Resin to Fabricate Highly Stretchable Structures. *Prog. Addit. Manuf.* **2023**, *8*, 1555–1571. [CrossRef]
38. Zheng, Q.; Xie, B.; Xu, Z.; Wu, H. A Systematic Printability Study of Direct Ink Writing towards High-Resolution Rapid Manufacturing. *Int. J. Extrem. Manuf.* **2023**, *5*, 035002. [CrossRef]
39. Marnot, A.; Dobbs, A.; Brettmann, B. Material Extrusion Additive Manufacturing of Dense Pastes Consisting of Macroscopic Particles. *MRS Commun.* **2022**, *12*, 483–494. [CrossRef]
40. M'Barki, A.; Bocquet, L.; Stevenson, A.; M'Barki, A.; Bocquet, L.; Stevenson, A. Linking Rheology and Printability for Dense and Strong Ceramics by Direct Ink Writing. *Sci. Rep.* **2017**, *7*, 6017. [CrossRef]
41. Rau, D.A.; Williams, C.B.; Bortner, M.J. Progress in Materials Science Rheology and Printability: A Survey of Critical Relationships for Direct Ink Write Materials Design. *Prog. Mater. Sci.* **2023**, *140*, 101188. [CrossRef]
42. Wei, P.; Cipriani, C.; Hsieh, C.M.; Kamani, K.; Rogers, S.; Pentzer, E. Go with the Flow: Rheological Requirements for Direct Ink Write Printability. *J. Appl. Phys.* **2023**, *134*, 100701. [CrossRef]
43. Li, Y.; Li, B. Direct Ink Writing 3D Printing of Polydimethylsiloxane-Based Soft and Composite Materials: A Mini Review. *Oxf. Open Mater. Sci.* **2022**, *2*, itac008. [CrossRef]
44. Loeb, C.K.; Nguyen, D.T.; Bryson, T.M.; Duoss, E.B.; Wilson, T.S.; Lenhardt, J.M. Hierarchical 3D Printed Porous Silicones with Porosity Derived from Printed Architecture and Silicone-Shell Microballoons. *Addit. Manuf.* **2022**, *55*, 102837. [CrossRef]
45. Slámečka, K.; Kashimbetova, A.; Pokluda, J.; Zikmund, T.; Kaiser, J.; Montufar, E.B.; Čelko, L. Fatigue Behaviour of Titanium Scaffolds with Hierarchical Porosity Produced by Material Extrusion Additive Manufacturing. *Mater. Des.* **2023**, *225*, 111453. [CrossRef]
46. Adhikari, S.; Torres, X.M.; Stockdale, J.R.; Legett, S.A.; Bezek, L.B.; Guajardo, J.A.; Pacheco, A.; Ramasamy, K.; Benedikt, B.; Lewis, M.; et al. 3D Printed Porous Silicone Polymer Composites Using Table Salt as a Sacrificial Template. *Mater. Adv.* **2024**, *5*, 8074–8085. [CrossRef]
47. Mazurek, P.; Ekbrant, B.E.F.; Madsen, F.B.; Yu, L.; Skov, A.L. Glycerol-Silicone Foams—Tunable 3-Phase Elastomeric Porous Materials. *Eur. Polym. J.* **2019**, *113*, 107–114. [CrossRef]
48. *ASTM D7175*; Standard Test Method for Determining the Rheological Properties of Asphalt Binder Using a Dynamic Shear Rheometer. ASTM International: West Conshohocken, PA, USA, 2018.
49. Zargar, R.; Nourmohammadi, J.; Amoabediny, G. Preparation, Characterization, and Silanization of 3D Microporous PDMS Structure with Properly Sized Pores for Endothelial Cell Culture. *Biotechnol. Appl. Biochem.* **2016**, *63*, 190–199. [CrossRef]
50. *ASTM D412*; Standard Test Methods for Vulcanized Rubber and Thermoplastic Elastomers—Tension. ASTM International: West Conshohocken, PA, USA, 2018.
51. Ozbolat, V.; Dey, M.; Ayan, B.; Povilianskas, A.; Demirel, M.C.; Ozbolat, I.T. 3D Printing of PDMS Improves Its Mechanical and Cell Adhesion Properties. *ACS Biomater. Sci. Eng.* **2018**, *4*, 682–693. [CrossRef]
52. Mazurek, P.; Hvilsted, S.; Skov, A.L. Green Silicone Elastomer Obtained from a Counterintuitively Stable Mixture of Glycerol and PDMS. *Polymer* **2016**, *87*, 1–7. [CrossRef]
53. *ASTM D575-91*; Standard Test Methods for Rubber Properties in Compression. ASTM International: West Conshohocken, PA, USA, 1991.
54. Gerling, G.J.; Hauser, S.C.; Soltis, B.R.; Bowen, A.K.; Fanta, K.D.; Wang, Y. A Standard Methodology to Characterize the Intrinsic Material Properties of Compliant Test Stimuli. *IEEE Trans. Haptics* **2018**, *11*, 498–508. [CrossRef]
55. Humairah, S.; Nabilah, N.; Abd, C.; Mahmud, J.; Mohammed, M.N.; Sapuan, S.M.; Ilyas, R.A.; Alkhatib, S.E.; Asyraf, M.R.M. Hyperelastic Properties of Bamboo Cellulosic Fibre—Reinforced Silicone Rubber Biocomposites via Compression Test. *Int. J. Mol. Sci.* **2022**, *23*, 6338. [CrossRef] [PubMed]
56. Del-Mazo-Barbara, L.; Ginebra, M. Rheological Characterisation of Ceramic Inks for 3D Direct Ink Writing: A Review. *J. Eur. Ceram. Soc.* **2021**, *41*, 18–33. [CrossRef]
57. Xu, K.; Li, D.; Shang, E.; Liu, Y. A Heating-Assisted Direct Ink Writing Method for Preparation of PDMS Cellular Structure with High Manufacturing Fidelity. *Polymers* **2022**, *14*, 1323. [CrossRef]

58. Tang, Z.; Jia, S.; Shi, X.; Li, B.; Zhou, C. Coaxial Printing of Silicone Elastomer Composite Fibers for Stretchable and Wearable Piezoresistive Sensors. *Polymers* **2019**, *11*, 666. [CrossRef]
59. Courtial, E.; Perrinet, C.; Colly, A.; Mariot, D.; Frances, J. Silicone Rheological Behavior Modification for 3D Printing: Evaluation of Yield Stress Impact on Printed Object Properties. *Addit. Manuf.* **2019**, *28*, 50–57. [CrossRef]
60. Lyu, Z.; Koh, J.J.; Lim, G.J.H.; Zhang, D.; Xiong, T.; Zhang, L.; Liu, S.; Duan, J.; Ding, J.; Wang, J.; et al. Direct Ink Writing of Programmable Functional Silicone-based Composites for 4D Printing Applications. *Interdiscip. Mater.* **2022**, *1*, 507–516. [CrossRef]
61. Ang, X.; Tey, J.Y.; Yeo, W.H.; Shak, K.P.Y. A Review on Metallic and Ceramic Material Extrusion Method: Materials, Rheology, and Printing Parameters. *J. Manuf. Process.* **2023**, *90*, 28–42. [CrossRef]
62. Danner, P.M.; Pleij, T.; Siqueira, G.; Bayles, A.V.; Venkatesan, T.R.; Vermant, J.; Opris, D.M. Polysiloxane Inks for Multimaterial 3d Printing of High-Permittivity Dielectric Elastomers. *Adv. Funct. Mater.* **2024**, *34*, 2313167. [CrossRef]
63. Lim, J.J.; Sim, J.H.; Tey, J.Y. Rheological Formulation of Room Temperature Vulcanizing Silicone Elastomer Ink for Extrusion-Based 3D Printing at Room Temperature. *J. Manuf. Process.* **2023**, *102*, 632–643. [CrossRef]
64. Ang, X.; Yuen, J.; Hong, W. 3D Printing of Low Carbon Steel Using Novel Slurry Feedstock Formulation via Material Extrusion Method. *Appl. Mater. Today* **2024**, *38*, 102174. [CrossRef]
65. Chen, Q.; Zhao, J.; Ren, J.; Rong, L.; Cao, P.F.; Advincula, R.C. 3D Printed Multifunctional, Hyperelastic Silicone Rubber Foam. *Adv. Funct. Mater.* **2019**, *29*, 1900469. [CrossRef]
66. Mazurek, P.; Brook, M.A.; Skov, A.L. Glycerol-Silicone Elastomers as Active Matrices with Controllable Release Profiles. *Langmuir* **2018**, *34*, 11559–11566. [CrossRef] [PubMed]
67. Kim, H.S.; Scheffold, F.; Mason, T.G. Entropic, Electrostatic, and Interfacial Regimes in Concentrated Disordered Ionic Emulsions. *Rheol. Acta* **2016**, *55*, 683–697. [CrossRef]
68. Brito, F.; Carvalho-guimar, D.; Correa, K.L.; De Souza, T.P.; Amado, J.R.R.; Riberio-Costa, R.M.; Silva-Júnior, J.O.C. A Review of Pickering Emulsions: Perspectives and Applications. *Pharmaceuticals* **2022**, *15*, 1413. [CrossRef]
69. Bhaktha, S.; Hegde, S.; Sathish, U.R.; Gandhi, N. Investigation of Tensile Properties of RTV Silicone Based Isotropic Magnetorheological. *MATEC Web Conf.* **2018**, *144*, 02015.
70. Zhu, X.; Zhang, X.; Yao, W.; Li, W. Split-Hopkinson Pressure Bar Test of Silicone Rubber: Considering Effects of Strain Rate and Temperature. *Polymers* **2022**, *14*, 3892. [CrossRef]
71. Waldemar, G.; Oscar, D.; César, J.; César, A. Effect of Porosity on the Tensile Properties of Low Ductility Aluminum Alloys. *Mater. Res.* **2004**, *7*, 221–229.
72. De Carolis, S.; Putignano, C.; Soria, L.; Carbone, G. International Journal of Mechanical Sciences Effect of Porosity and Pore Size Distribution on Elastic Modulus of Foams. *Int. J. Mech. Sci.* **2024**, *261*, 108661. [CrossRef]
73. Shi, L.U.O.; Guo, D.; Bin, D.A.I.; Meng, Y.; Fang, L.I.U. Study on the Cell Structure and Mechanical Properties of Methyl Vinyl Silicone Rubber Foam Materials. *Adv. Mater. Res.* **2014**, *1005*, 297–306. [CrossRef]
74. Peng, L.; Lei, L.; Liu, Y.; Du, L. Improved Mechanical and Sound Absorption Properties of Open Cell Silicone Rubber Foam with NaCl as The. *Materials* **2021**, *14*, 195. [CrossRef]
75. Wang, H.; Yan, R.; Cheng, H.; Zou, M.; Wang, H.; Zheng, K. Hollow Glass Microspheres/Phenolic Syntactic Foams with Excellent Mechanical and Thermal Insulate Performance. *Front. Chem.* **2023**, *11*, 1216706. [CrossRef] [PubMed]
76. Kumar, V.; Alam, M.N.; Yewale, M.A.; Park, S.S. Multifunctional Aspects of Mechanical and Electromechanical Properties of Composites Based on Silicone Rubber for Piezoelectric Energy Harvesting Systems. *Polymers* **2024**, *16*, 2058. [CrossRef] [PubMed]
77. Upadhyay, A.; Ullas, A.V. Compressive Properties of Poly (Dimethylsiloxane)–Hollow Glass Microballoons Syntactic Foams. *Cell. Polym.* **2022**, *41*, 243–251. [CrossRef]
78. Zhang, K.; Zhang, X.; Gao, Q.; Chan, M.; Zhang, S.; Li, J.; Liao, W.H. Ultrahigh Energy-Dissipation and Multifunctional Auxetic Polymeric Foam Inspired by Balloon Art. *Compos. Part A Appl. Sci. Manuf.* **2023**, *167*, 107435. [CrossRef]
79. Yoshimura, K.; Nakano, K.; Nishiwaki, T.; Iwama, Y.; Murata, M. Effects of Graded Porous Structures on the Mechanical and Electrical Properties of Ketjenblack/Silicone-Rubber Composites. *Sensors Actuators A Phys.* **2021**, *332*, 113099. [CrossRef]
80. AZoM Silicone Rubber. Available online: https://www.azom.com/article.aspx?ArticleID=920 (accessed on 31 August 2024).

Disclaimer/Publisher's Note: The statements, opinions and data contained in all publications are solely those of the individual author(s) and contributor(s) and not of MDPI and/or the editor(s). MDPI and/or the editor(s) disclaim responsibility for any injury to people or property resulting from any ideas, methods, instructions or products referred to in the content.